Int. J. Electrochem. Sci., 13 **(2018)** 8042 – 8055, doi: 10.20964/2018.08.69

International Journal of
ELECTROCHEMICAL
SCIENCE
www.electrochemsci.org

An Investigation of Mn−Ce−Based Conversion Coating on LZ91 Magnesium Alloy

Shun-Yi Jian[1,*], *Ko-Lun Chang*[2]

[1] Department of Chemical & Materials Engineering, Chung Cheng Institute of Technology, National Defense University, Dasi, Taoyuan 335, Taiwan, ROC
[2] National Synchrotron Radiation Research Center, 101 Hsin-Ann Road, Hsinchu 30076, Taiwan, ROC
[*]E-mail: ftvko@yahoo.com.tw

Received: 18 April 2018 / *Accepted:* 12 June 2018 / *Published:* 5 July 2018

Most of the magnesium alloys are relatively reactive and tend to suffer corrosion. Consequently, surface modifications are performed to enhance the corrosion resistance and paint adhesion of the base magnesium alloys. This work discuss with the non-chromate conversion coating on LZ91 magnesium alloy. The conversion coating treatment is conducted in an acidic cerium/permanganate solution with adding the different acidity regulators. These additives can adjust the pH value of the solution and influence the formation of anti-corrosion coatings on LZ91 substrate. The microstructure and composition of the conversion coating are characterized using SEM, EDS and cross-sectional TEM. The potentiodynamic polarization test, electrochemical impedance spectroscopy and salt spray test results show that the corrosion resistance of LZ91 alloy is markedly improved by the acidic cerium/permanganate conversion coating. The corrosion protection efficiency is related with the acidity regulator in the conversion solution. The film thickness also depends upon the acidity regulator used. Besides, micro-cracks are more obvious on the coating formed in the phosphoric acid bath. Therefore, the coating formed in the sulfuric acid bath does provide the LZ91 plate better corrosion protection when compared to the coating formed in the phosphoric acid bath.

Keywords: LZ91 Magnesium alloy; Conversion coating; Corrosion resistance; EIS; Microstructure

1. INTRODUCTION

Magnesium is the eighth most abundant element on the earth and its alloys have excellent physical and mechanical properties such as low density, high specific strength, good damping effect, and excellent electromagnetic shielding characteristics [1, 2]. However, the corrosion resistance of magnesium alloys is poor. Several surface treatments have been developed to improve the corrosion resistance. Among the various treatments, chemical conversion treatment is an efficient and low cost

technology to provide anti-corrosion and paint adhesion properties on magnesium alloys.

The hexavalent chromate conversion coating (CCC) has been widely used to promote the corrosion resistance of magnesium alloys during the past years [3-5]. The hexavalent chromate conversion coating of self-healing functionality has proven to provide superior corrosion resistance for magnesium alloys. The self-healing functionality provides an additional benefit that the coating itself can regenerate a new one when damaged. Nevertheless, owing to the high toxicity, the use of Cr (VI) species has been prohibited according to the RoHS directive (Restriction of Hazardous Substances Directive).

Phosphate/Permanganate conversion coating has been studied for substituting chromate conversion coating in recent years [6-16]. In our previous study, a phosphate/permanganate conversion coating was processed on an AZ31 alloy in strong acidic solution (pH < 2), which was found to promote the growth rate of the coating [17]. Meanwhile, instead of a porous and cellular structure of $Mg(OH)_2$, a more compact layer of MnO_2 and good corrosion resistance was observed. Therefore, the conversion solution containing one primary component ($KMnO_4$) and another minor additive ($Ce(NO_3)_3$) in strongly acidic electrolyte, including the phosphoric acid (H_3PO_4) bath and sulfuric acid (H_2SO_4) bath was used to treat the LZ91 Mg alloy in this study. The effects of different treatment solutions on the microstructure and composition of the conversion coating were investigated. The microstructure and composition of the conversion coating were characterized using scanning electron microscopy (SEM) and transmission electron microscopy (TEM). The corrosion resistance of the coating was characterized by potentiodynamic polarization tests, electrochemical impedance spectroscopy (EIS) and salt spray teat (SST) analyses. The results show that the coating treated in the H_2SO_4 bath could provide excellent corrosion protection on a LZ91 sheet.

2. EXPERIMENTAL

2.1. Conversion coating treatment

A cold-rolled LZ91 plate was used as the test materials, which contained 9.73 wt.% Li, Zn wt.% 0.85, and Mg balance. The plate with 1.5 mm thick was cut into the size of 50 mm × 25 mm. Then the cut substrates were mechanically ground with emery paper from 400 to 1200 grit. Finally, the pretreated substrates were rinsed with deionized water and dried with an air stream.

Table 1. The composition and pH of the conversion solution used in this study (Time: 30 s, Temperature: 25℃ and pH=1.5).

The conversion solution	$KMnO_4$	$Ce(NO_3)_3$	H_3PO_4	H_2SO_4
phosphoric acid bath	0.1 M	0.02 M	adjust pH value	-
sulfuric acid bath	0.1 M	0.02 M	-	adjust pH value

The composition of the manganese-based conversion solution was shown in Table 1. In addition to reducing the solution pH with the addition of phosphoric acid (H_3PO_4) as commonly studied previously, another acidity regulator (sulfuric acid; H_2SO_4) was also used for comparison. The conversion coatings were prepared by immerging LZ91 Mg alloy samples in the phosphoric acid solution and sulfuric acid solution at 25 ℃ and pH=1.5, respectively. The treatment time was fixed at 30 s. After conversion coating treatment, the LZ91 plate was thoroughly rinsed in deionized water and then left to dry in room temperature air overnight [6, 18-19].

2.2. Microstructural Analyses

The surface morphology of the conversion coating was investigated using scanning electron microscopy (SEM, JEOL JSM-7800F Prime FEG-SEM). The thickness of the conversion coating was measured on the cross-sections of the coupons via transmission electron microscopy (TEM, FEI Tecnai G2 F20) and the crystalline structure of the coating was identified using the selected area electron diffraction (SAED). On the other hand, cross-sectional TEM was employed to investigate the detailed microstructure of the coating. The cross-sectional sample was prepared by a Focused Ion Beam and Electron Beam System (FIB, SII 3050SE). Finally, the composition of the conversion coating was measured using energy-dispersive spectrometry (EDS) equipped in SEM and TEM, respectively.

2.3. Properties of the conversion coating

The adhesion of the conversion coating was measured by standard tape test according to the ASTM D3359-97. The electrochemical characteristics of the coating were investigated using a Potentiostat (VERSASTAT4, Princeton Applied Research) in a three-electrode cell consisting of a platinum sheet as the counter electrode and a saturated calomel electrode (SCE) as the reference electrode. The measurements were conducted in a solution containing 3.5 wt.% sodium chloride (NaCl) at 25℃. The potentiodynamic polarization curves were obtained by scanning at a rate of 1 mV s^{-1} from −300 mV to +500 mV with respect to the OCP. The impedance spectra were acquired using a sinusoidal wave with amplitude of 5 mV over the frequency range between 10^{-2} Hz and 10^5 Hz. EIS data were analyzed by fitting to proper electrical equivalent circuit using Zimpwin software (version 3.21). Finally, the corrosion behavior of the bare and coated LZ91 alloys was also evaluated after 48 h salt spray test in accordance with ASTM B117-03 and ASTM D610-08 standard. All adhesion tests, electrochemical tests and SSTs were conducted in triplicate to confirm the reproducibility of results.

3. RESULTS

3.1. Surface Morphology and Composition of the Coatings

Fig. 1 showed the surface morphology of the coating formed in the phosphoric acid bath and

sulfuric acid bath, respectively. Polishing grooves left after mechanical polishing remained visible on the coupon after both treatments. Meanwhile, micro-cracks were more obvious on the coating formed in the phosphoric acid bath. Figure 1(b) shows the results in larger, evenly-distributed micro-cracks with wider openings. Relatively small micro-cracks were observed on the coating formed in the sulfuric acid bath. Micro-cracks are frequently observed on the magnesium alloys after phosphating [6, 10, 18-20] or acid pickling [21-22]. They are ascribed to result from dehydration during the post-immersion drying process [10, 18, 20-21].

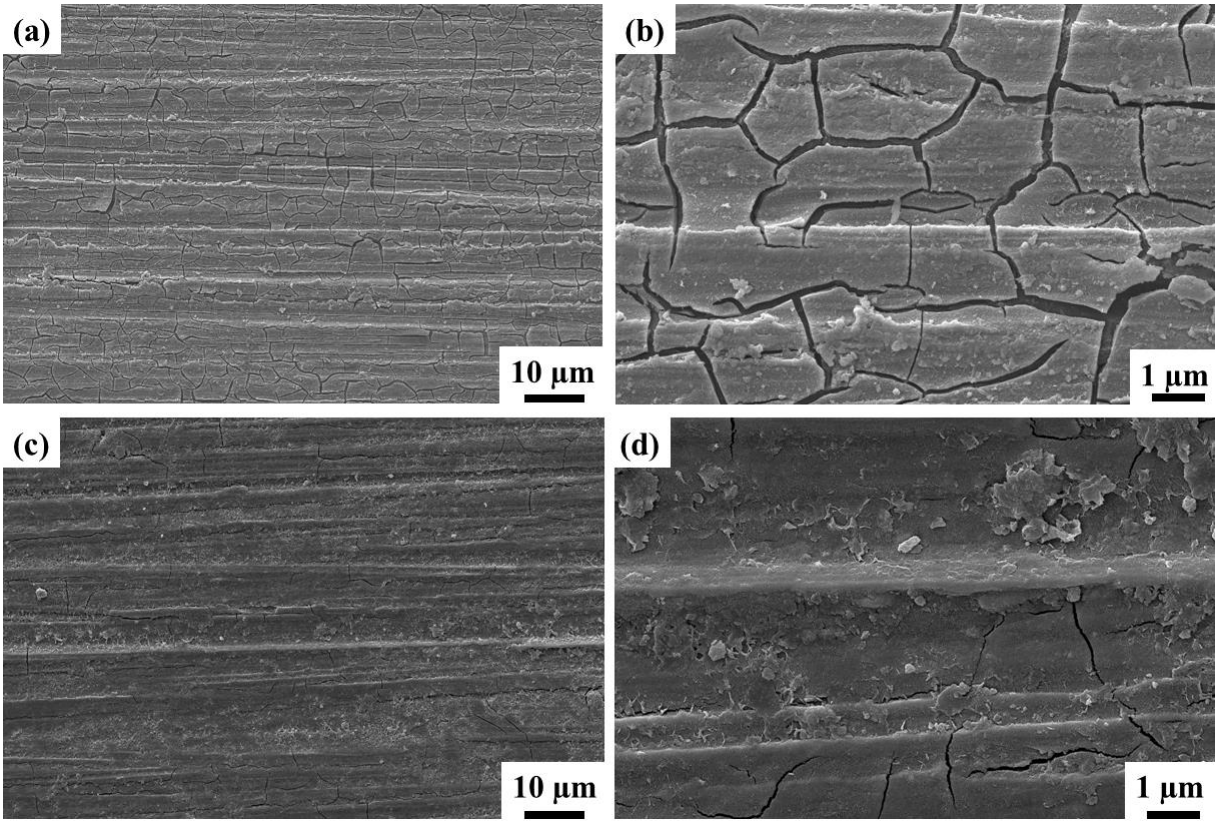

Figure 1. Surface morphology of the LZ91 alloy treated in the phosphoric acid bath (a) and (b), as well as of that treated in the sulfuric acid bath (c) and (d).

Table 2. The chemical composition of the conversion coating on LZ91 plates measured by the EDS equipped in the SEM.

	Element - Atomic%						
	O	Mg	Ce	Mn	P	S	Total
phosphoric acid bath	42.3 (±1.8)	42.5 (±2.2)	1.6 (±0.3)	8.4 (±0.4)	5.2 (±0.2)	-	100
sulfuric acid bath	43.3 (±1.1)	38.8 (±1.2	3.1 (±0.3)	14.4 (±0.4	-	0.4 (±0.2)	100

Table 2 shows the composition of the various coating detected by EDS in SEM. The both

coatings mainly contained magnesium (Mg), oxygen (O), Cerium (Ce) and manganese (Mn) species, a similar trend regarding its change in composition. Further the coatings formed in the sulfuric acid bath resulted in insignificant comprise in the sulfur (S) contents, while a slight increase in Mn and O and a slight decrease in Mg (compare to the phosphoric acid bath).

3.2. Cross-Sectional TEM

A more detailed cross-sectional morphology was shown using TEM (bright field image). Fig. 2 shows the cross-sectional TEM of the coating formed in the phosphoric acid bath. The thickness of the conversion coating was about 260 nm (indicated by the double arrows). Compare with the conventional phosphate-permanganate conversion coating on Mg alloy, which consists of the multilayered structure [18, 20, 23], the coating of the present study presents a single-layered structure as shown in Fig. 2(a). Fig. 3 showed the cross-sectional TEM of the coating formed in the sulfuric acid bath. In comparison to Fig. 2, the coating formed in the sulfuric acid bath presents a thicker thickness (600~650 nm) and is relatively compact.

On the contrary, micro-cracks were more obvious on the coating formed in the phosphoric acid bath (Fig. 1). Thus, it depends on the composition of the coating.

Table 3. The chemical composition of the conversion coating on LZ91 plates measured by the EDS equipped in the TEM.

	Element - Atomic%						
	O	Mg	Ce	Mn	P	S	Total
phosphoric acid bath (point A)	70.7 (±1.1)	14.4 (±0.5)	0.2 (±0.1)	6.3 (±0.4)	8.4 (±0.8)	-	100
sulfuric acid bath (point B)	75.9 (±1.2)	10.5 (±1.1)	3.1 (±0.2	10.3 (±0.8)	-	0.2 (±0.1)	100

Table 3 shows the results of the EDS spectra taken from each film (at the middle site) observed in the TEM. In addition to Mg and O species, the film contained a significant amount of Mn and P species, suggesting that the coating formed in the phosphoric acid bath was composed of Mn oxide, Mg/P chemical compound and Mg hydroxide (as the minor phase). Moreover, the signal intensity of Mn from the coating in the phosphoric acid solution decreases substantially and there was only a small amount of Ce. It is consistent with the EDS analyses of the SEM. Finally, both selected-area electron diffraction (SAED) patterns comprised diffused halos indicating that those coatings had a poor crystallinity (Fig. 2(b) and Fig. 3(b)).

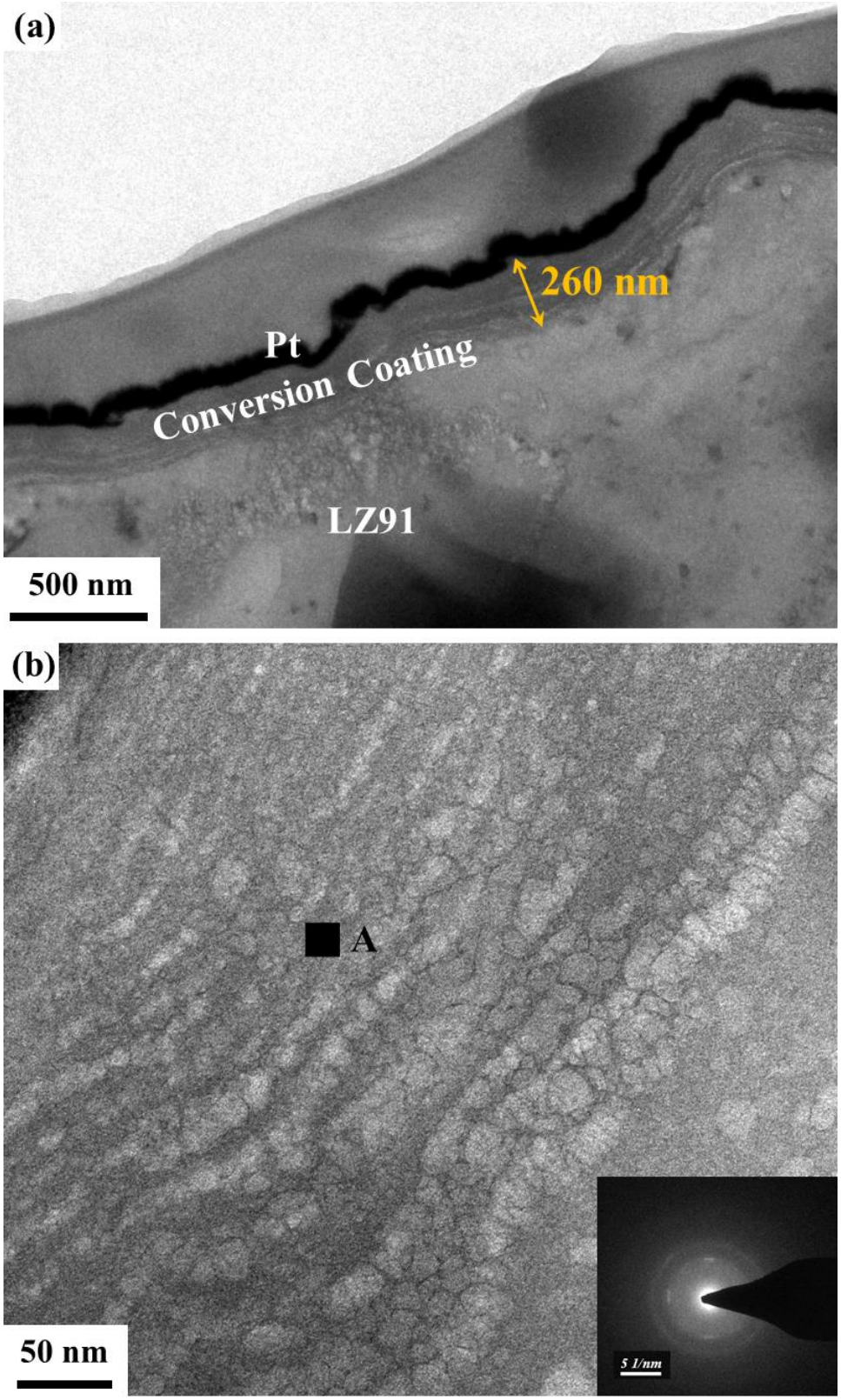

Figure 2. Cross-sectional TEM characterization of the LZ91 alloy treated in the phosphoric acid bath for 30 s.

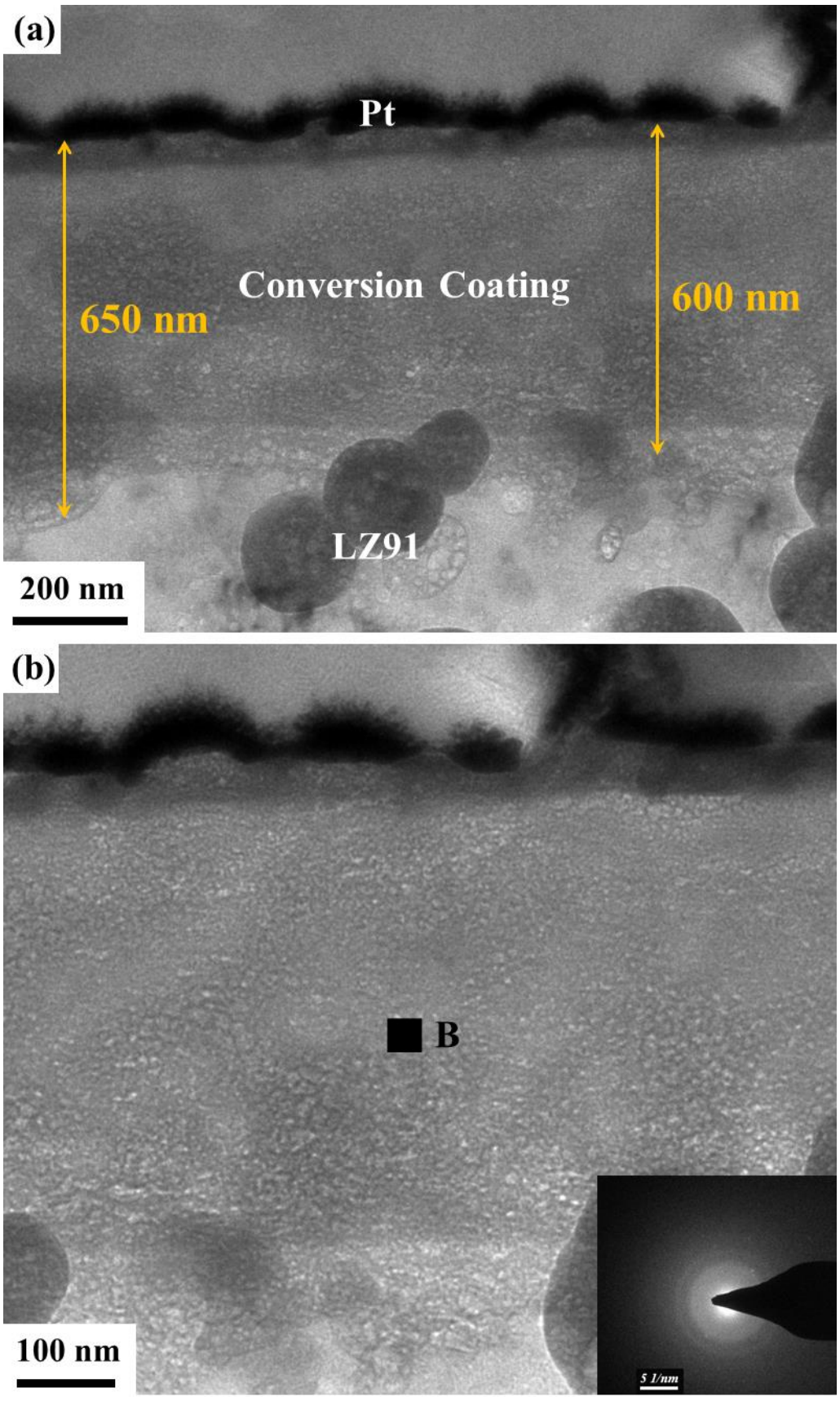

Figure 3. Cross-sectional TEM characterization of the LZ91 alloy treated in the sulfuric acid bath for 30 s.

3.3. Corrosion resistance of electrochemical analysis

Potentiodynamic polarization and EIS measurement were conducted to evaluate the corrosion resistance of the various coated LZ91 plates in 3.5 wt.% NaCl solution. The polarization curves of bare LZ91 and the coated LZ91 plates are shown in Fig. 4.

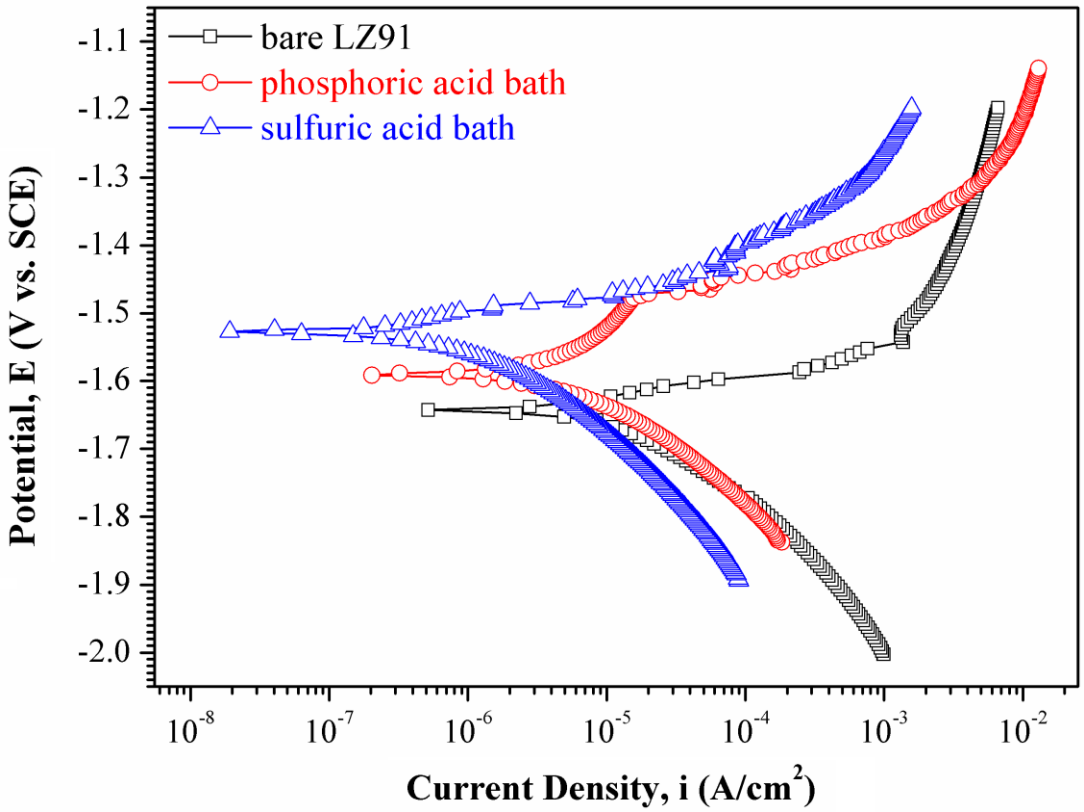

Figure 4. Potentiodynamic polarization curves of bare LZ91 and the conversion coated LZ91 samples in 3.5 wt.% NaCl solution.

The electrochemical values of the corrosion potential (E_{corr}) and the corrosion current density (I_{corr}) are listed in Table 4.

Table 4. Results of potentiodynamic polarization tests of bare LZ91 and the conversion coated LZ91 Mg alloy in 3.5 wt.% NaCl solution.

	Bare LZ91	Phosphoric acid bath	Sulfuric acid bath
E_{corr} (V_{SCE})	-1.62 (±6.88 x 10^{-3})	-1.59 (±5.76 x 10^{-3})	-1.53 (±8.52 x 10^{-3})
I_{corr} (μA/cm^2)	15.6 (±2.75)	7.58 (±1.28)	1.05 (±0.36)
β_a (V/decade)	0.035 (±1.08 x 10^{-4})	0.109 (±3.38 x 10^{-4})	0.324 (±1.01 x 10^{-4})
β_c (V/decade)	-0.155 (±4.81 x 10^{-4})	-0.117 (±3.63 x 10^{-4})	-0.076 (±2.36 x 10^{-4})

Compared to the bare LZ91, a shift in the corrosion potential toward the active direction was

observed for the LZ91 with the coatings formed in the phosphoric acid bath or sulfuric acid bath. This difference is likely to be associated with cracks formed during the drying process [10, 23]. And, the higher corrosion potential of the coating formed in the sulfuric acid bath compared to that formed in the phosphoric acid bath can be related to the presence of Mn oxide. This result is consistent with the EDS analyses of the SEM and TEM [14-15]. However, the phosphoric acid bath coated LZ91 had a larger corrosion current density than the sulfuric acid bath coated LZ91. Apparently, the coating formed in the phosphoric acid bath did not afford the LZ91 plate corrosion protection. In contrast, the coating formed in the sulfuric acid bath reduced the corrosion density of the LZ91 plate, as compared to the bare LZ91 [19, 24-26].

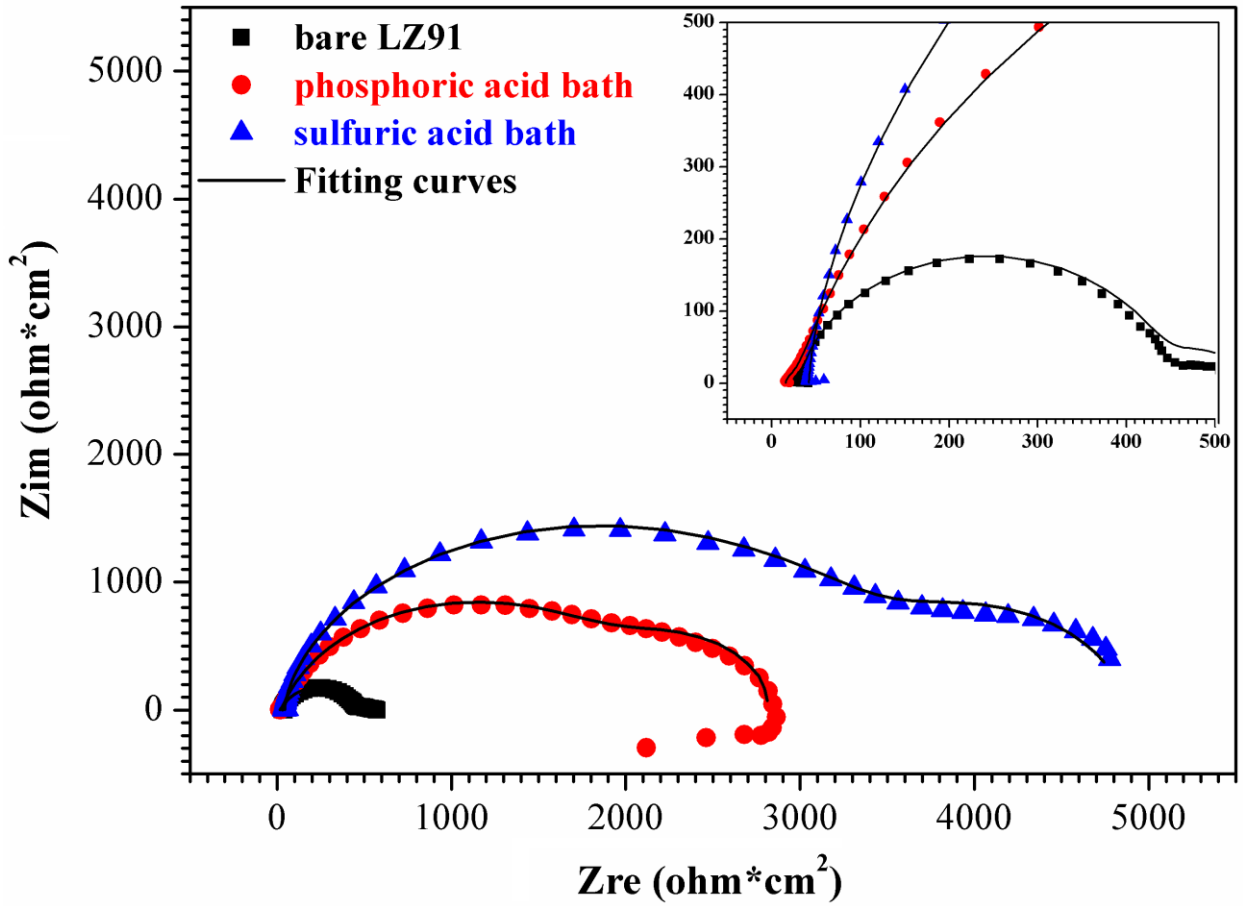

Figure 5. The Nyquist plot ant the fitted curves of the various LZ91 samples.

Fig. 5 shows the Nyquist plots and the fitting curves of bare LZ91 and the various coated LZ91 plates. All Nyquist plots displayed two well-defined capacitive loops appearing at high and medium frequencies, respectively. In addition, they couple with low frequency inductive loop except the LZ91 treated in the sulfuric acid bath. A comparison of the Nyquist plots shows: (1) The capacitive loops were larger in diameter for the LZ91 with the conversion coatings compared to the bare counterpart, indicating that the conversion coatings improved the corrosion resistance of LZ91 alloys because the size of the capacitive loop is a characteristic of the impedance of the specimen. (2) The treatment in the sulfuric acid bath led to an increase in the diameter of the capacitive loop. Accordingly, the LZ91

plates treated in the sulfuric acid bath had the largest impedance, signifying the conversion coating improved its protective capability in the test solution. (3) The low frequency impedance of the LZ91 plates treated in the phosphoric acid bath was lower than that of the coated LZ91 plates treated in the sulfuric acid bath. The reduced impedance of the former specimens is possibly related to the coating adjacent to the substrate was loosely, which was evident by TEM (Fig. 2(b)).

The EIS data was further simulated using the equivalent circuit shown in Figure 6, where R_s represents the solution resistance. Song investigated that a porous $Mg(OH)_2$ with lower protection capability was formed on magnesium in corrosion tested solutions, where corrosion proceeded in the film-free areas [27-28]. Baril successfully characterized the EIS of pure magnesium in Na_2SO_4 solutions and found that the high frequency impedance was associated with the charge transfer reaction at the film-free areas and the medium-frequency impedance was related to the diffusion of Mg^{2+} in porous $Mg(OH)_2$ [29].

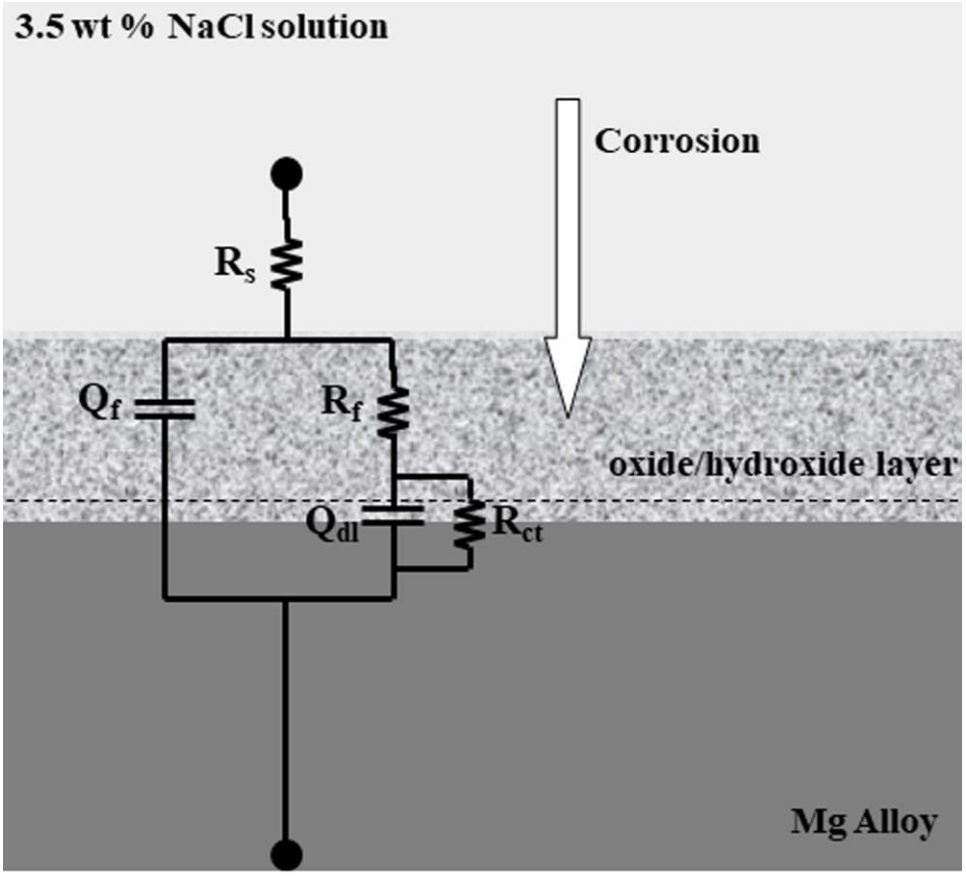

Figure 6. The equivalent circuit models for the simulation of the Nyquist plots on the various LZ91 samples.

Therefore, the impedance response of the bare LZ91 can be fitted by the equivalent circuit shown in Fig. 6, where the constant phase element (Q_f) (in the ZSimpWin program, Q stands for CPE in the circuit) and resistance (R_f) of the film model the properties of the corrosion product (presumably $Mg(OH)_2$); a parallel combination of a constant phase element representing double layer capacitance (Q_{dl}) and charge transfer resistance (R_{ct}) models the characteristic of the film-free areas.

Table 5. The fitted value of equivalent electric circuit extrapolated from EIS simulations for LZ91 substrate and various conversion coated AZ91D plates tested.

	Bare LZ91	Phosphoric acid bath	Sulfuric acid bath
R_s (ohm.cm^2)	30.0 (±3.51)	26.1 (±2.32)	41.8 (±4.49)
Q_f (s^n.μohm^{-1}.cm^{-2})	45.3 (±2.76)	36.2 (±2.13)	10.1 (±0.78)
Q_f - n	0.88 (±8.58 x 10^{-3})	0.88 (±8.27 x 10^{-3})	0.91 (±6.58 x 10^{-3})
R_f (ohm.cm^2)	4.24 x 10^2 (±3.66 x 10^1)	2.39 x 10^3 (±1.52 x 10^2)	2.53 x 10^3 (±1.84 x 10^2)
Q_{dl} (s^n. μohm^{-1}.cm^{-2})	7.58 x 10^3 (±1.38 x 10^3)	1.50 x 10^3 (±96.6)	2.36 x 10^2 (±12.1)
Q_{dl} - n	0.86 (±8.50 x 10^{-3})	0.90 (±4.43 x 10^{-2})	0.91 (±4.60 x 10^{-2})
R_{ct} (ohm.cm^2)	9.57 x 10^1 (±1.03 x 10^1)	5.53 x 10^2 (±5.46 x 10^2)	2.65 x 10^3 (±1.59 x 10^3)

Table 5 summarizes the simulated values of the electric elements using the ZSimpWin 3.21 software for various LZ91 specimens. On the other hand, because the conversion coating effectively increased the size of the two capacitive loops, the Nyquist plot of the conversion coated LZ91 can be characterized by two capacitive loops attributed to the coating effect and charge transfer [30-34], where Q_f and R_f model the properties of the conversion coating; Q_{dl} and R_{ct} model the characteristic of the coating/substrate interface.

3.4. Adhesion and salt spray test

Table 6. The adhesion test results of the various Conversion Coatings.

Conversion bath	Classification	Percent Area Removed
phosphoric acid bath	5 B	0 %, None
sulfuric acid bath	5 B	0 %, None

In order to evaluate the adhesion of the various conversion coatings, cross hatch adhesion tests results were used to verify the degree of coating peeled off, as shown in Table 6. The results showed that all coatings have the great adhesion with a classification of 5 B. It illustrates that the coatings

remained completely after the cross hatch adhesion tests and no severe damage occurred.

Table 7. The percentage of corrosion area and rust grade on the various coated plates after 12, 24, 36 and 48 h salt spray test.

	Corrosion area fraction (%) and Rust grade			
	12 h	24 h	36 h	48 h
phosphoric acid bath	＜10 (4)	＜16 (3)	＜16 (3)	＜33 (2)
sulfuric acid bath	＜1 (6)	＜1 (6)	＜1 (6)	＜3 (5)

The results of the SST for the coated LZ91 alloys are shown in Fig. 7, and the quantification of the corrosion area and rust grade were given in Table 7.

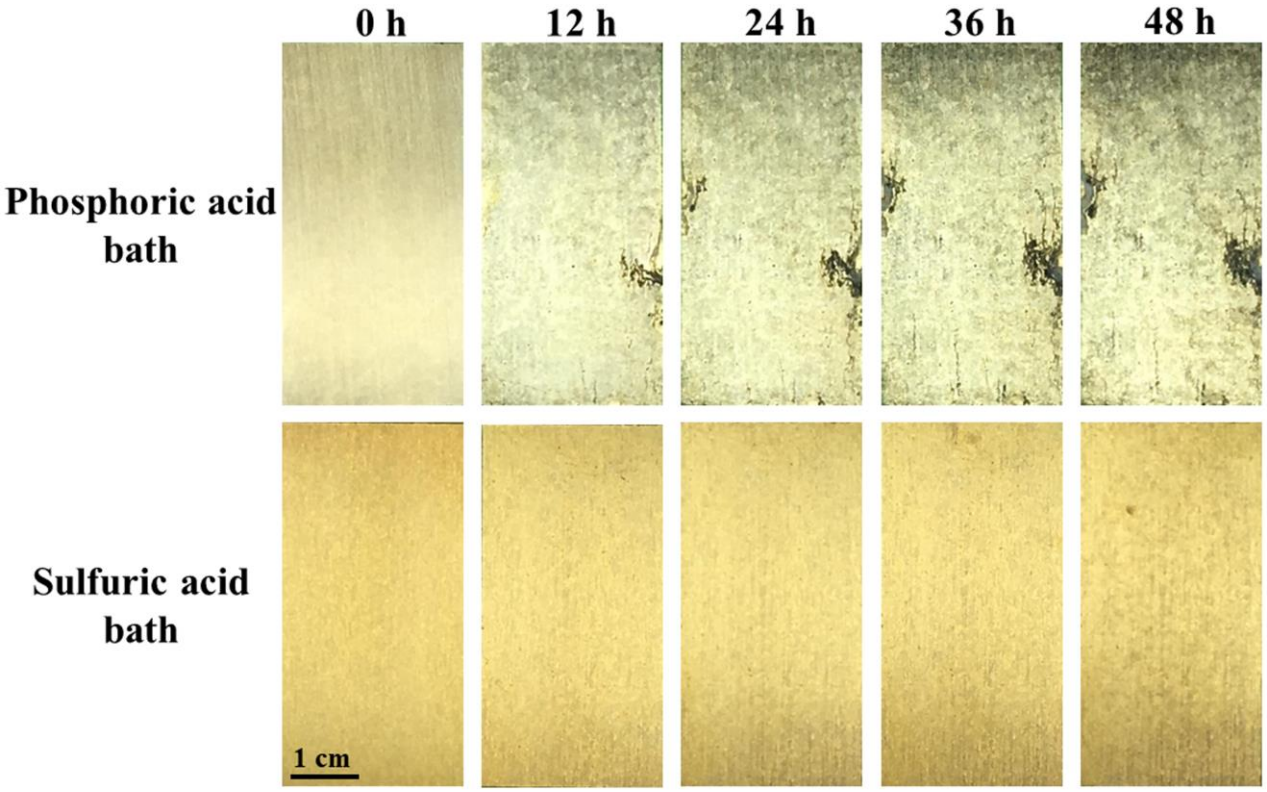

Figure 7. Optical images of the coated LZ91 plates formed in the phosphoric acid and sulfuric acid bath after salt spray test for various durations respectively.

The corroded area fraction after 12 h of the SST was approximately 100 % for the bare LZ91 (not shown here). The data of the specimens was recorded each 12 hours during the salt spray test for the purpose to study the corrosion process. For the coated LZ91, there was less than 1 % corrosion area for the sample treated in the sulfuric acid bath in the first 12 hours except the sample treated in the phosphoric acid bath, which was shown around 10 % corrosion area on it. After 24 hour, all specimens

increased around 0.5 % and 3 % corrosion area respectively. And at the end of the test, LZ91 plate treated in the sulfuric acid bath had less than 3 % corrosion area, which was the based demand for the corrosion resistance in the industrial applications.

4. CONCLUSIONS

The different acid baths induces a complex effect on both the composition and microstructure of the coating. Specifically, a thinner coating is formed in the sulfuric acid bath and contains smaller cracks which exhibits a better corrosion resistance than that formed in the phosphoric acid bath. The effect of the acidic solution on the microstructure and corrosion resistance of the conversion coating on LZ91 magnesium alloys has been detailed. The conclusions are listed as follows:

1. The coated LZ91 plates are mainly composed of Mg, O, and Mn species by using EDS equipped in TEM. The Mn content of the coating formed in the phosphoric acid and sulfuric acid bath are approximately 6.3 and 10.3 at.%, respectively.
2. The average thickness of the coatings formed in the phosphoric acid and sulfuric acid bath is 260 and 625 nm, respectively. Cracks are formed due to the dehydration of the coating during drying after conversion process.
3. The corrosion current densities of the coated LZ91 formed in the phosphoric acid and sulfuric acid bath are 7.58 μA/cm^2 and 1.05 μA/cm^2, respectively. Comparison of each resistance element (R_f and R_{ct}), the coated LZ91 formed in the sulfuric acid bath had largest R_f and R_{ct}, which is consistent with the results that the conversion coating became compact as the immersion proceeded.
4. The coated substrate exhibited a better corrosion resistance than the uncoated one based on the SST results. Especially, the coated LZ91 formed in the sulfuric acid bath has higher corrosion resistance than other specimens.
5. From all the results, it is suggested that the SO_4^{2-} ions in the conversion solution plays a less important role. In contrast, the PO_4^{3-} ions promotes the formation of insoluble or sparingly soluble phosphate precipitates in the conversion coating.

ACKNOWLEDGEMENT
This study was financially supported by the Ministry of Science and Technology of Taiwan, Republic of China, under Grant No. MOST 107-2623-E-606-004-D. In addition, thanks to Ms. C. Y. Chien of Ministry of Science and Technology (National Taiwan University) for the assistance in FIB experiments.

References

1. J. E. Gray, B. Luan, *J. Alloys Comp.*, 336 (2002) 88.
2. M. Avedesian, H. Baker, *ASM Specialty Handbook*, 3 (1999) 138.
3. R. E. Van de Leest, *Werkstoffe und Korrosion*, 29 (1978) 648.
4. E. Cuynen, P. V. Espen, G. Goeminne, H. Terryn, *J. Anal. At. Spectrom.*, 14 (1999) 483.

5. E. Cuynen, G. Goeminne, P. V. Espen, H. Terryn, *Surf. Interface Anal.*, 30 (2000) 589.
6. D. Hawke and D. L. Albright, *Metal Finishing*, 93 (1995) 34.
7. H. Umehara, S. Terauchi and M. Takaya, *Mater. Sci. Forum*, 273 (2000) 350.
8. H. Umehara, M. Takaya and Y. Kojima, *Mater. Trans.*, 42 (2001) 1691.
9. H. Umehara, M. Takaya and S. Terauchi, *Surf. Coat. Technol.*, 666 (2003) 169.
10. K. Z. Chong and T. S. Shih, *Mater. Chem. Phys.*, 80 (2003)191.
11. I. Azkarate, P. Cano, A. Del Barrio, M. Insausti, P. S. Coloma, *Magnesium Alloys and their Appl.*, (2006) 475.
12. M. Zhao, S. Wu, J. Luo, Y. Fukuda and H. Nakae, *Surf. Coat. Technol.*, 200 (2006) 5407.
13. H. Zhang, G. Yao, S. Wang, Y. Liu, H. Luo, *Surf. Coat. Technol.*, 202(9) (2008) 1825.
14. A. S. Hamdy, H. M. Hussien, *Int. J. Electrochem. Sci.*, 8 (2013) 11386.
15. A. S. Hamdy, H. M. Hussien, *Int. J. Electrochem. Sci.*, 9 (2014) 2682.
16. F. P. Hu, Y. Zhang, Q. W. Zeng, N. Jia, J. Qin, X. Zhang, S. Z. Wang, J. M. He, W. D. Xie, *Mater. Corros.*, 67 (2016) 1128.
17. S.Y. Jian, Y.R. Chu, C.S. Lin, *Corros. Sci.*, 93 (2015) 301.
18. C. S. Lin, C. Y. Lee, W. C. Li, Y. S. Chen, G. N. Fang, *J. Electrochem. Soc.*, 153 (2006) B90.
19. F. Zucchi, A. Frignani, V. Grassi, G. Trabanelli, C. Monticelli, *Corros. Sci.*, 49 (2007) 4542.
20. W. Zhou, D. Shan, E. H. Han and W. Ke, *Corr. Sci.*, 50 (2008) 329.
21. U. C. Nwaogu, C. Blawert, N. Scharnagl, W. Dietzel and K. U. Kainer, *Corros. Sci.*, 51 (2009) 2544.
22. M. Zhao, S. Wu, P. An and J. Luo, *Mater. Chem. Phys.*, 103 (2007) 475.
23. Y.L. Lee, Y.R. Chu, W.C. Li, C.S. Lin, *Corros. Sci.*, 70 (2013) 74.
24. Y. Guan, J.G. Liu, C.W. Yan, *Int. J. Electrochem. Sci.*, 6 (2011) 4853.
25. S. Chen, S. Zhang, X. Ren, S. Xu, L. Yin, *Int. J. Electrochem. Sci.*, 10 (2015) 9073.
26. Q.Y. Xiong, J.P. Xiong, Y. Zhou, F. Yan, *Int. J. Electrochem. Sci.*, 12 (2017) 4238.
27. G. Song, A. Atrens, D. ST John, J. Nairn, Y. Li, *Corros. Sci.*, 39 (1997) 855.
28. G. Song, A. Atrens, D. ST John, X. Wu, J. Nairn, *Corros. Sci.*, 39 (1997) 1981.
29. G. Baril, G. Galicia, C. Deslouis, N. Pebere, B. Tribollet, V. Vivier, *J. Electrochem. Soc.*, 154 (2007) C108.
30. J. Chen, Y. Song, D. Shan, E. H. Han, *Corros. Sci.*, 65 (2012) 268.
31. G. Baril, N. Pebere, *Corros. Sci.*, 43 (2001) 471.
32. Y. Zhang, C. Yan, F. Wang, W. Li, *Corros. Sci.*, 47 (2005) 2816.
33. Y. G. Ko, S. Namgung, D. H. Shin, *Surf. Coat. Technol.*, 205 (2010) 2525.
34. D. Seifzadeh, A. G. Haghighat, *Indian J. Chem. Technol.*, 20 (2013) 210.